Mathematical Modelling and Control

http://www.aimspress.com/journal/mmc

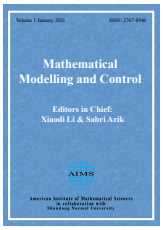

MMC, 3(4): 400–415.
DOI: 10.3934/mmc.2023032
Received: 27 May 2023
Revised: 27 August 2023
Accepted: 27 August 2023
Published: 27 December 2023

Research article

Hidden chaotic mechanisms for a family of chameleon systems

Xue Zhang[1], Bo Sang[1,*], Bingxue Li[1], Jie Liu[1], Lihua Fan[1] and Ning Wang[2]

[1] School of Mathematical Sciences, Liaocheng University, Liaocheng 252059, China

[2] School of Microelectronics and Control Engineering, Changzhou University, Changzhou 213159, China

* **Correspondence:** Email: sangbo_76@163.com.

Abstract: Chameleon chaotic systems are nonlinear dynamical systems whose chaotic attractors can transform between hidden and self-excited types by tuning system parameters to modify equilibrium points. This paper proposes a novel family of chameleon chaotic systems, which can exhibit three types of chaotic attractors: self-excited attractors with a nonhyperbolic equilibrium, hidden attractors with a stable equilibrium, and hidden attractors with no equilibrium points. Bifurcation analysis uncovers the mechanisms by which self-excited and hidden chaotic attractors arise in this family of chameleon systems. It is demonstrated that various forms of chaos emerge through period-doubling routes associated with changes in the coefficient of a linear term. An electronic circuit is designed and simulated in Multisim to realize a hidden chaotic system with no equilibrium points. It is demonstrated that the electronic circuit simulation is consistent with the theoretical model. This research has the potential to enhance our comprehension of chaotic attractors, especially the hidden chaotic attractors.

Keywords: Hopf bifurcation; period-doubling route; bifurcation diagram; hidden chaotic attractor

1. Introduction

Chaos arises in dynamical systems governed by nonlinear deterministic equations. It is characterized by sensitivity to initial conditions, topological transitivity, and the presence of dense periodic orbits. Nonlinearity in the underlying equations allows for stretching, folding, and reinjection of trajectories in phase space, resulting in complex long-term evolution [1]. Chaos systems have found widespread applications in various domains, with mathematical modeling playing a crucial role. These domains include biology [2], economics [3], physics [4] and many others. Based on the mathematical framework, we can simulate the functioning and mechanisms of systems within these domains. In recent years, there has been growing interest in experimental investigations of chaotic attractors [5, 6].

Around 2010, the classification of attractors into hidden and self-excited types was introduced in several papers by Leonov, Kuznetsov et al. [7–9]. Since then, many researchers have further examined properties of hidden attractors and methods to find them, publishing a series of related works [10, 11]. An attractor is classified as a self-excited attractor if its basin of attraction intersects with any open neighborhood of an unstable equilibrium point. On the other hand, it is called a hidden attractor if its basin of attraction is not connected with any unstable equilibrium point. Hidden attractors are significant in engineering applications because they can lead to unexpected and potentially disastrous responses to perturbations in structures such as bridges or airplane wings [12]. Therefore, identifying and analyzing hidden attractors is crucial for ensuring the safety and reliability of these structures. Over the past few years, the identification of hidden attractors has given rise to the development of the theory of hidden oscillations [13]. In 2023, Wang et al. [14] demonstrated that chaotic systems can display various types of symmetries, such as involutional, circulant,

and conditional (approximate) symmetries. It enhanced our understanding of self-excited and hidden attractors in chaotic systems with various symmetries.

Self-excited attractors can be located by a standard procedure. This involves choosing an initial state in a neighborhood of an unstable equilibrium, allowing the system to evolve for a transient period, observing the trajectory, and tracing the state of oscillation. Many well-known dynamical systems, such as the Lorenz, Chen, Lu and Tigan systems, can exhibit self-excited attractors [15]. Hidden attractors are challenging to find as their basins of attraction can be small and their dimensions lower than the system's. The identification of hidden attractors in multidimensional systems demands specialized numerical procedures to pinpoint initial conditions within their attraction basins and compute trajectories. The joint application of homotopy and numerical continuation systematically identifies suitable initial data to expose hidden attractors [16]. In the pursuit of uncovering hidden attractors, researchers have proposed the use of perpetual points as a potential tool [17]. Perpetual points are characterized by the property of having zero acceleration but nonzero velocity. In certain dynamical systems, perpetual points have been shown to be effective in revealing coexisting hidden attractors [18]. However, it has been demonstrated in [19] that perpetual points do not offer a reliable general method for finding hidden attractors.

Hidden attractors have been observed in a wide variety of dynamical systems, including systems without equilibrium points [20], systems with only stable equilibrium points [21], and systems with an infinite number of equilibria situated on curves or surfaces [22]. These different types of systems represent distinct challenges for the analysis and control of their dynamical behavior. Pham et al. explored instances of interconversion between these three types, as described in [23–25].

A chameleon chaotic system is a type of system that exhibits a chaotic attractor which can switch between being a hidden attractor and a self-excited attractor, based on the parameter values. In 2017, Jafari et al. [26] proposed a simple chameleon chaotic system that exhibited three types of hidden attractors as well as self-excited attractors. This system demonstrates how the behavior of a dynamical system depends on the values of its parameters, highlighting the importance of studying hidden attractors for a better understanding of complex systems. In 2018, Wu et al. [27] demonstrated that the Hamilton energy feedback scheme can effectively control the dynamic behavior of the chameleon chaotic flow. In 2021, Mobayen et al. [28] introduced nine chameleon chaotic systems by adding two parameters to a 3D chaotic system with quadratic nonlinearities. The analysis of these systems revealed three categories of hidden attractors and a self-excited attractor.

In dissipative systems, multistability refers to the coexistence of several possible attractors for a given set of parameters [29]. Each attractor has its own basin of attraction–the set of initial conditions that will eventually converge to that attractor. The basins of attraction of different attractors are separated by basin boundaries [30]. Multistable dynamical systems are highly sensitive to noise, initial conditions, and parameters [31]. In 2015, Sharma et al. [32] presented the method of linear augmentation to control multistability in hidden chaotic systems, which is significant for engineering applications needing specific outputs. In 2023, Ahmadi et al. [33] introduced a new non-autonomous mega-extreme multistable chaotic system with complex dynamics. Also in 2023, Moalemi et al. [34] developed a novel mega-stable system with attractors mimicking real-life object shapes.

A Hopf bifurcation is a local bifurcation where an equilibrium of a dynamical system changes stability as a parameter is varied. It occurs at points where the system has a non-hyperbolic equilibrium connected with a pair of purely imaginary eigenvalues. There are no zero eigenvalues, and additional transversality conditions are met. The bifurcation can be supercritical or subcritical, resulting in either a stable or an unstable limit cycle within an invariant two-dimensional manifold, respectively. The latter scenario is potentially dangerous, because stable large-amplitude limit cycles can coexist with the stable equilibrium point [35]. In 2017, Stankevich et al. [36] revisited the dynamics of the Chua circuit and studied the scenario relating subcritical Hopf bifurcations near equilibria to the emergence of hidden attractors. It was conjectured in [36] that a subcritical Hopf bifurcation of an equilibrium in a bounded autonomous system generally

leads to hidden attractors. Various nonlinear dynamical systems have provided substantial evidence supporting this conjecture, as shown by Zhao et al. [37], Liu et al. [38] and Li et al. [39]. In 2023, Kumarasamy et al. [40] revealed new routes to hidden attractors in nonlinear systems through saddle-node bifurcations of periodic orbits.

This paper introduces and investigates a family of chameleon systems, uncovering the mechanisms behind the emergence of self-excited chaotic attractors and hidden chaotic attractors. In Section 2, we present a family of chameleon systems with linear, affine, and quadratic functions in the variable z. Depending on the form of the function, the system can exhibit a self-excited chaotic attractor with a nonhyperbolic equilibrium, a hidden chaotic attractor with a stable equilibrium, or a hidden chaotic attractor with no equilibrium. In Section 3, the bifurcation diagrams are plotted and analyzed individually to uncover the distinct routes to chaos for each of the three systems. Section 4 is devoted to Hopf bifurcation analysis. In Section 5, the Multisim software is utilized to perform circuit design and simulation for a hidden chaotic system with no equilibrium points. Finally, concluding remarks are presented in Section 6.

2. A family of chameleon systems

In this paper, we consider a family of quadratic systems

$$\begin{cases} \dfrac{dx}{dt} = y, \\ \dfrac{dy}{dt} = -x + y\,z, \\ \dfrac{dz}{dt} = \mu(z) - 5\,x\,y + x\,z, \end{cases} \tag{2.1}$$

where $\mu(z)$ is an element of the set $\mathcal{P}$, consisting of polynomials in $\mathbb{R}[z]$ with degree 1 or 2. The divergence function of the system is given by

$$\mathrm{Div}(f(x,y,z)) = x + z + \mu'(z), \tag{2.2}$$

where $f(x,y,z)$ denotes the vector field associated to the system. System (2.1) is dissipative in a certain region where the system has a negative average divergence. This means that, on average, the volume element contracts with the flow as time advances. The simplest example is the region defined by

$$x + z + \mu'(z) < 0.$$

In order to understand the dynamical behavior of the system through theoretical analysis and numerical simulations, we introduce the following three polynomials:

$$\mu_1(z) = -b\,z, \tag{2.3}$$

$$\mu_2(z) = a - b\,z, \tag{2.4}$$

$$\mu_3(z) = a - b\,z + c\,z^2. \tag{2.5}$$

In Section 3, these polynomials will be utilized to gain insight into the routes to chaos that the system takes as the parameter b varies.

Based on the forthcoming observations, we come to know that system (2.1) is a chameleon system, indicating that the system has the capability to generate self-excited and hidden chaotic attractors. The precise manifestation depends on the nature of the function $\mu(z)$.

2.1. *Self-excited chaotic flow with a nonhyperbolic equilibrium:* $\mu(z) = -z$

Consider the system (2.1) with $\mu(z) = \mu_1(z)$ and $b = 1$, where $\mu_1(z)$ is defined in (2.3). It has a unique equilibrium at the origin. The eigenvalues of the linear part of the system at this point are $\lambda_{1,2} = \pm\mathrm{i}$ and $\lambda_3 = -1$. This nonhyperbolic equilibrium is determined to be unstable based on the Hopf bifurcation analysis in Section 4. The system displays a self-excited chaotic attractor (blue) in the form of a thin ring-shaped structure, as depicted in Figure 1. A cross section of the attractor in the y-z plane (at $x = 0$) is shown in Figure 2, revealing the chaotic behavior through the presence of an infinite number of scattered points on the cross section. The Lyapunov exponents of the attractor were calculated using the Wolf algorithm [41], employing the ode113 solver with a time-step of 0.05 for a total simulation duration of 40000 units. The attractor has Lyapunov exponents of $(0.0680483, 0.000398604, -1.55594)$ and a Kaplan-Yorke dimension of 2.04399. The positive maximum Lyapunov exponent indicates the presence of chaos in the system. In addition, the sum of all the Lyapunov exponents is negative, indicating that the system is dissipative.

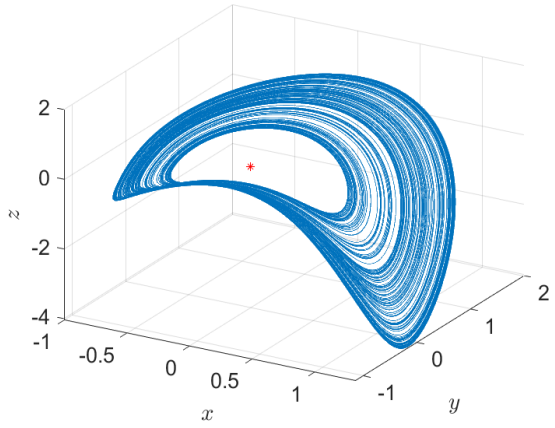

Figure 1. Self-excited chaotic attractor of system (2.1) with $\mu(z) = -z$, visualized by an orbit starting from the initial conditions $(x(0), y(0), z(0)) = (0, 1, 0)$ near the unstable equilibrium at the origin (marked with a red star).

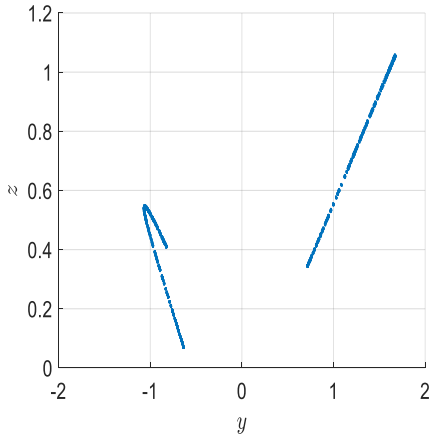

Figure 2. Cross section in the y-z plane (at $x = 0$) of the chaotic attractor of system (2.1) with $\mu(z) = -z$ and initial conditions $x(0) = z(0) = 0, y(0) = 1$.

2.2. *Hidden chaotic flow with a stable equilibrium: $\mu(z) = -0.01 - z$*

Consider system (2.1) with

$$\mu(z) = \mu_2(z) \text{ and } a = -0.01,\ b = 1,$$

where $\mu_2(z)$ is defined in (2.4). It has a unique equilibrium at

$$x = 0,\ y = 0 \text{ and } z = -0.01$$

with the eigenvalues

$$\lambda_{1,2} = \frac{-1 \pm \sqrt{39999}\mathrm{i}}{200}, \qquad \lambda_3 = -1.$$

This singularity is a stable node-focus. All initial conditions in the vicinity of the equilibrium spiral towards the equilibrium point. Besides the point attractor, the system also has a hidden chaotic attractor, as highlighted in Figure 3. The Lyapunov exponents of this attractor are $(0.0585773, 0.0000779879, -1.54072)$. Thus the Kaplan-Yorke dimension is 2.03807. There is a decrease in the maximal Lyapunov exponent when moving from the self-excited chaotic attractor in subsection 2.1 to the hidden chaotic attractor in subsection 2.2.

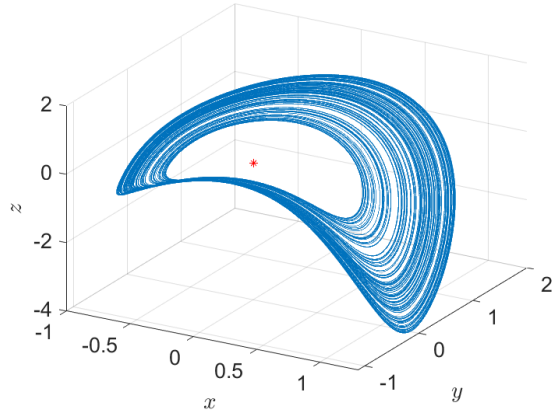

Figure 3. Hidden chaotic attractor of system (2.1) with $\mu(z) = -0.01 - z$ and initial conditions $x(0) = z(0) = 0, y(0) = 1$. Red star: stable equilibrium at $x = 0, y = 0, z = -0.01$.

For system (2.1) with $\mu(z) = -0.01 - z$, a cross section of the basins of attraction of two attractors in the $y(0)$-$z(0)$ plane at $x(0) = 0$ is illustrated in Figure 4. It shows the regions of initial conditions that lead to either the hidden chaotic attractor or the stable equilibrium point $x = y = 0$, $z = -0.01$. The magenta region corresponds to the hidden chaotic attractor, shown in the cross section as black lines. The red region corresponds to the stable equilibrium point.

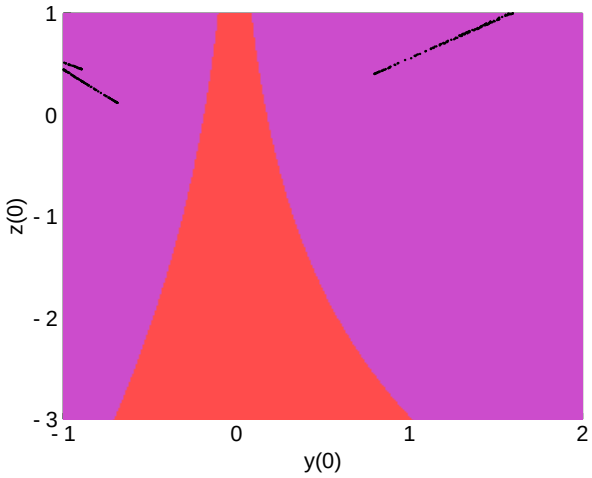

Figure 4. Cross section of the basins of attraction of two attractors in the $y(0)$-$z(0)$ plane at $x(0) = 0$ for system (2.1) with $\mu(z) = -0.01 - z$. Initial conditions within the magenta region lead to the emergence of the hidden chaotic attractor, shown in the cross section as black lines. In contrast, initial conditions within the red region lead to the stable equilibrium point.

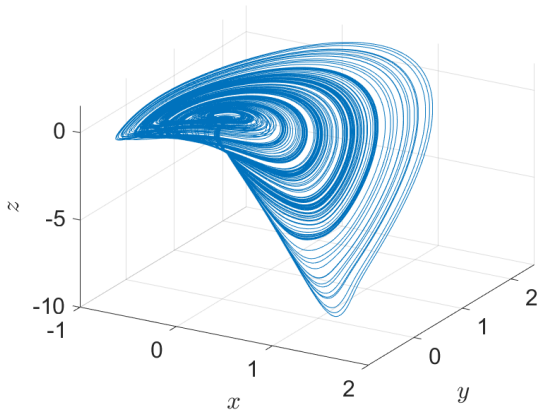

Figure 5. Hidden chaotic attractor of system (2.1) with $\mu(z) = 0.1 - 0.195z + 0.1z^2$ and initial conditions $x(0) = z(0) = 0, y(0) = 1$.

2.3. *Hidden chaotic flow without equilibrium:* $\mu(z) = 0.1 - 0.195\,z + 0.1\,z^2$

Consider system (2.1) with

$$\mu(z) = \mu_3(z) \text{ and } a = 0.1,\ b = 0.195,\ c = 0.1,$$

where $\mu_3(z)$ is defined in (2.5). It does not contain any equilibrium points. With initial conditions

$$x(0) = 0,\ y(0) = 1,\ z(0) = 0,$$

a hidden chaotic attractor of the system can be found in Figure 5.

By computations, this attractor is found to have Lyapunov exponents $(0.0329968, 0.000201782, -0.866228)$, leading to a Kaplan-Yorke dimension of 2.03833. A cross section of the attractor in the y-z plane at $x = 0$ is illustrated in Figure 6, revealing the chaotic behavior through the presence of an infinite number of scattered points on the cross section.

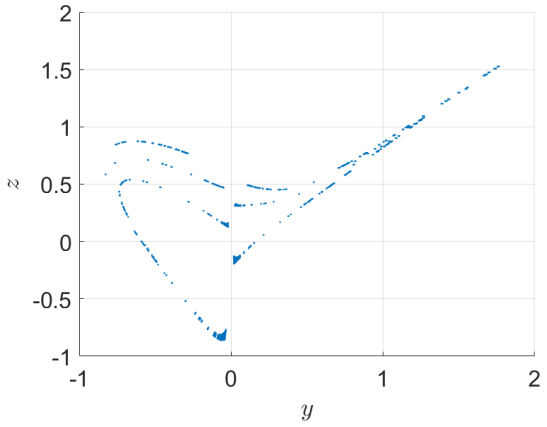

Figure 6. Cross section of the hidden chaotic attractor of system (2.1) in the y-z plane at $x = 0$, with $\mu(z) = 0.1 - 0.195z + 0.1z^2$ and the initial conditions $x(0) = z(0) = 0, y(0) = 1$.

3. Bifurcation analysis

In order to provide clarity on the chaotic behavior presented in Section 2, we will discuss the relationship between the parameter b and the long-term behavior of the system. We will employ bifurcation diagrams to investigate the mechanisms underlying the chaotic dynamics.

3.1. Self-excited dynamics: $\mu(z) = -b\,z$ and $b \in [0.4, 1.6]$

For system (2.1), we assume that $\mu(z)$ takes the form $\mu(z) = -b\,z$ with $b \in [0.4, 1.6]$. In this case, the system has a unique equilibrium at origin with eigenvalues $\lambda_{1,2} = \pm\mathrm{i}, \lambda_3 = -b$. The singularity is unstable, as concluded from the Hopf bifurcation analysis in Section 4. As a result, we need to study the self-excited dynamics in the system.

From Figure 1, we have observed a self-excited chaotic attractor at $b = 1$. To understand its underlying mechanism, we construct a bifurcation diagram Figure 7 by varying parameter b, while maintaining fixed initial conditions $x(0) = z(0) = 0$ and $y(0) = 1$. This allows us to monitor how the behavior of x evolves with respect to the parameter b. As the parameter b increases from $b = 0.4$ to $b = 1.6$, the initial limit cycle undergoes a period-doubling route to chaos. Periodic windows can be found for some low periods, such as period-3 ($b \in [1.02, 1.10]$) and period-5 (near $b = 1.505$). The Lyapunov exponent spectrum of the system with respect to the parameter b is displayed in Figure 8. The qualitative behavior of the attractor can be specified by determining the signs of the Lyapunov exponents. The triple $(0, -, -)$ corresponds to a limit cycle, while $(+, 0, -)$ corresponds to a chaotic attractor. The Lyapunov exponent spectrum shown in Figure 8 is consistent with the bifurcation diagram shown in Figure 7.

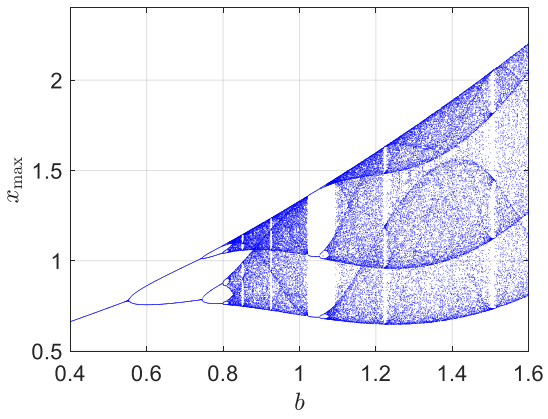

Figure 7. Bifurcation diagram of x for system (2.1) versus the parameter $b \in [0.4, 1.6]$ with $\mu(z) = -bz$ and initial conditions $x(0) = z(0) = 0, y(0) = 1$.

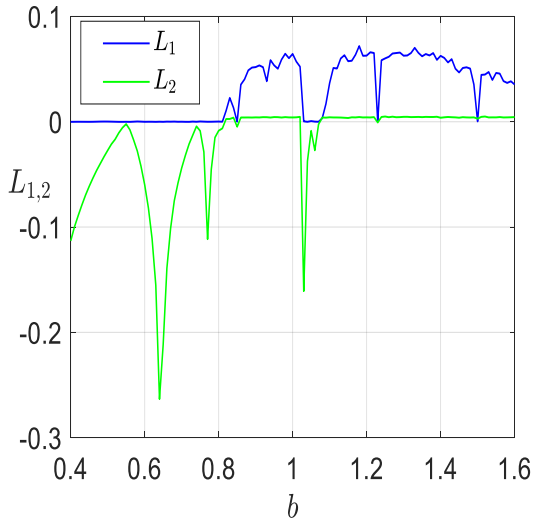

(a) The first two Lyapunov exponents $L_{1,2}$.

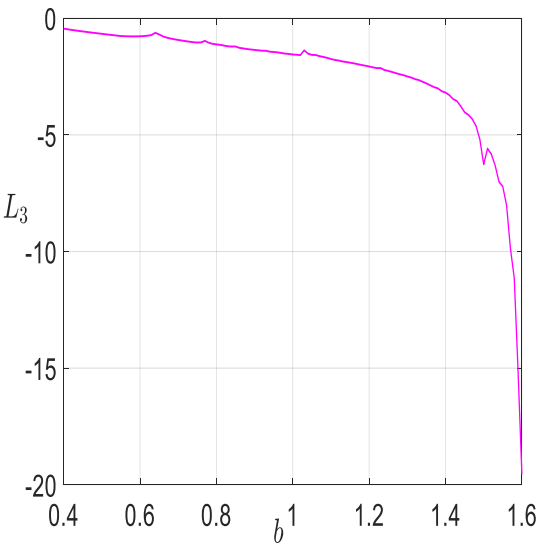

(b) The third Lyapunov exponent L_3.

Figure 8. Lyapunov exponent spectrum of system (2.1) versus the parameter $b \in [0.4, 1.6]$ with $\mu(z) = -bz$ and initial conditions $x(0) = z(0) = 0, y(0) = 1$.

3.2. Hidden dynamics with a stable equilibrium: $\mu(z) = -0.01 - b\,z$ and $b \in [0.4, 1.6]$

Let us consider system (2.1) with $\mu(z) = -0.01 - bz$, allowing the parameter b to vary within the range of $[0.4, 1.6]$. It has a unique equilibrium at

$$x = y = 0, \quad z = -(100\,b)^{-1}$$

with eigenvalues given by

$$\lambda_{1,2} = (200\,b)^{-1}\left(-1 \pm \sqrt{(200\,b)^2 - 1}\,\mathrm{i}\right), \quad \lambda_3 = -b.$$

As all these eigenvalues have negative real parts due to the constraint that b falls within the range of $[0.4, 1.6]$, the singularity is a stable node-focus. When $b = 1$, there exhibits a hidden chaotic attractor, coexisting with a stable node-focus located at

$$x = y = 0, \quad z = -100^{(-1)},$$

as depicted in Figure 3.

With the initial conditions $x(0) = z(0) = 0$, $y(0) = 1$, Figure 9 gives the bifurcation diagram of x with respect to the parameter b. The bifurcation diagram starts with steady-state response (stable equilibrium) in the interval $[0.4, 0.45)$. At the critical value $b = 0.45$, a discontinuous transition takes place, shifting from a point attractor to a period-1 limit cycle. As b increases further, the branch of limit cycles experiences a period-doubling route to hidden chaotic behavior.

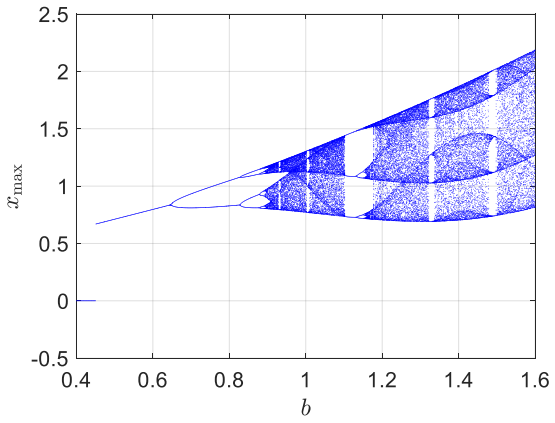

Figure 9. Bifurcation diagram of x for system (2.1) versus the parameter $b \in [0.4, 1.6]$ with $\mu(z) = -0.01 - bz$ and initial conditions $x(0) = z(0) = 0, y(0) = 1$.

At the value $b = 0.45$, it is noteworthy that the system displays bistable behavior. Bistable behavior refers to a phenomenon in a dynamical system where there are two distinct attractors that the system can settle into. In Figure 10, orbits (in blue and red) respectively converge to a stable equilibrium point and a stable limit cycle from the initial conditions of $(0.5, 0, 0)$ and $(-0.5, 0, 0)$.

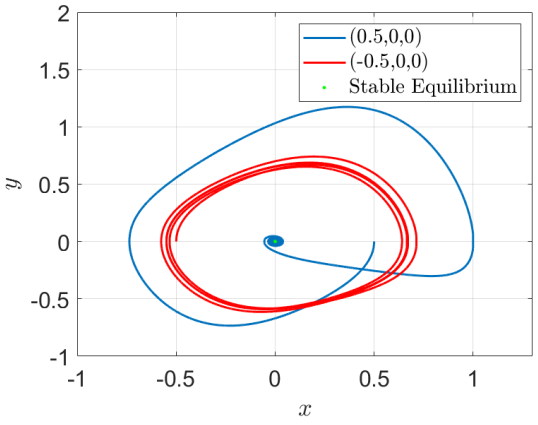

Figure 10. Two orbits of system (2.1) with $\mu(z) = -0.01 - 0.45z$. The blue orbit of the initial conditions $(x(0), y(0), z(0)) = (0.5, 0, 0)$ settles into a stable equilibrium point, while the red one of the initial conditions $(x(0), y(0), z(0)) = (-0.5, 0, 0)$ tends towards a stable limit cycle.

The Lyapunov exponent spectrum of the system with respect to the parameter b is depicted in Figure 11. The type of the attractor can be determined by analyzing the signs of the Lyapunov exponents. The pattern $(-, -, -)$ corresponds to a stable equilibrium, $(0, -, -)$ corresponds to a limit cycle, and $(+, 0, -)$ corresponds to a chaotic attractor. The Lyapunov exponent spectrum shown in Figure 11 aligns with the bifurcation diagram shown in Figure 9.

3.3. From self-excited attractor to hidden attractor via b decrease: $\mu(z) = 0.1 - b\,z + 0.1\,z^2$, where $b \in [0, 1]$

Let us consider system (2.1) with

$$\mu(z) = 0.1 - b\,z + 0.1\,z^2,$$

where b is a parameter ranging within the interval $[0, 1]$. We will study the influence of the parameter b on the dynamical behavior of the system.

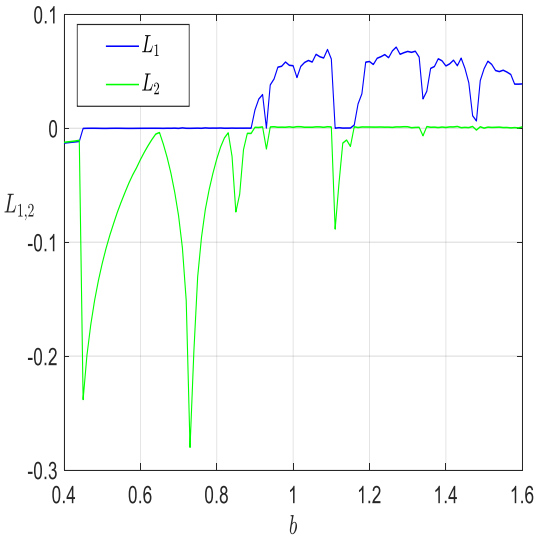

(a) The first two Lyapunov exponents $L_{1,2}$.

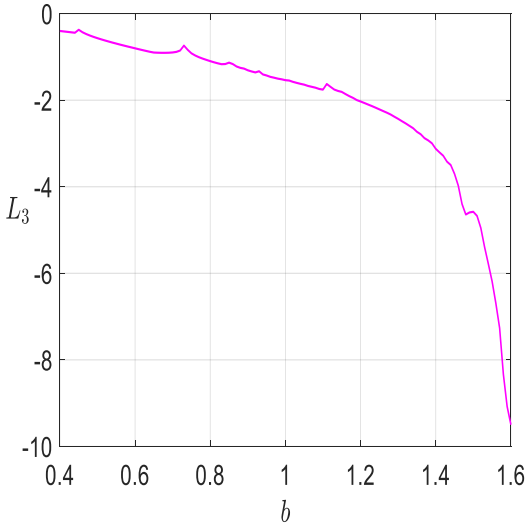

(b) The third Lyapunov exponent L_3.

Figure 11. Lyapunov exponent spectrum of system (2.1) versus the parameter $b \in [0.4, 1.6]$ with $\mu(z) = -0.01 - bz$ and initial conditions $x(0) = z(0) = 0, y(0) = 1$.

3.3.1. Local analysis

If $b \in [0, 0.2)$, then the system has no equilibrium point. If $b = 0.2$, there exists a single equilibrium at $P : (0, 0, 1)$. If $b \in (0.2, 1]$, then the system has two equilibria at

$$P_{1,2} : (0, 0, 5\,b \pm \sqrt{25\,b^2 - 1}).$$

At $b = 0.2$, the Jacobian matrix of the system at P has three distinct eigenvalues:

$$\lambda_1 = 0,\ \lambda_{2,3} = \frac{1 \pm \mathrm{i}\sqrt{3}}{2}.$$

Since there are two eigenvalues with positive real parts and one zero eigenvalue, the equilibrium P is nonhyperbolic and unstable, with a one-dimensional center manifold $W^c(P)$ and a two-dimensional unstable manifold $W^u(P)$.

Proposition 3.1. *For system* (2.1) *with*

$$\mu(z) = 0.1 - 0.2\,z + 0.1\,z^2,$$

the center manifold and unstable manifold at the equilibrium $P(0, 0, 1)$ *are give by:*

$$W^c(P) : x = y = 0, \tag{3.1}$$

$$W^u(P) : z = 1 - y + x + \frac{1}{10}y^2 - \frac{11}{10}xy - \frac{39}{20}x^2 + \cdots, \tag{3.2}$$

respectively.

Proof. We need to consider the following system

$$\begin{cases} \dfrac{dx}{dt} = y, \\ \dfrac{dy}{dt} = -x + y\,z, \\ \dfrac{dz}{dt} = 0.1 - 0.2\,z + 0.1\,z^2 - 5\,x\,y + x\,z, \end{cases} \tag{3.3}$$

which has a unique equilibrium located at $P(0, 0, 1)$. The Jacobian matrix of the system at P has three distinct eigenvalues:

$$\lambda_1 = 0,\ \lambda_{2,3} = \frac{1 \pm \mathrm{i}\sqrt{3}}{2}.$$

Since the eigenvector corresponding to λ_1 is $(0, 0, 1)^T$, the center space at P is the z-axis: $x = y = 0$. Furthermore, the z-axis is invariant under the flow of system (3.3). Thus we can conclude that the center manifold of system (3.3) at P can be denoted by

$$W^c(P) : x = y = 0.$$

Using the transformation

$$\begin{cases} x = \dfrac{v}{2} + \dfrac{\sqrt{3}}{2} w, \\ y = -\dfrac{v}{2} + \dfrac{\sqrt{3}}{2} w, \\ z = u + v + 1, \end{cases} \tag{3.4}$$

system (3.3) becomes

$$\begin{cases} \dfrac{du}{dt} = & \sqrt{3}wu + \sqrt{3}wv + \dfrac{1}{5}vu + \dfrac{27}{20}v^2 \\ & + \dfrac{1}{10}u^2 - \dfrac{15}{4}w^2, \\ \dfrac{dv}{dt} = & \dfrac{1}{2}v + \dfrac{\sqrt{3}}{2}w + \dfrac{1}{2}v^2 - \dfrac{\sqrt{3}}{2}wv \\ & + \dfrac{1}{2}uv - \dfrac{\sqrt{3}}{2}uw, \\ \dfrac{dw}{dt} = & -\dfrac{\sqrt{3}}{2}v + \dfrac{1}{2}w - \dfrac{\sqrt{3}}{6}v^2 + \dfrac{1}{2}wv \\ & - \dfrac{\sqrt{3}}{6}uv + \dfrac{1}{2}uw. \end{cases} \tag{3.5}$$

For later convenience, let (U, V, W) represent the vector field associated to system (3.5).

Suppose that the unstable manifold of system (3.5) is parametrised by

$$u = h(v, w) = a_1 v^2 + a_2 vw + a_3 w^2 + \cdots, \tag{3.6}$$

then,

$$\frac{\partial h}{\partial v} V(h, v, w) + \frac{\partial h}{\partial w} W(h, v, w) = U(h, v, w), \tag{3.7}$$

where $h = h(v, w)$.

Equating terms of like powers in v, w up to the second order, we find a solution of (a_1, a_2, a_3), which yields

$$h(v, w) = -\frac{3v^2}{16} - \frac{41\sqrt{3}wv}{40} - \frac{177w^2}{80} + \cdots. \tag{3.8}$$

Going back to the original coordinates, the unstable manifold of system (3.3) is approximately

$$z = 1 - y + x + \frac{1}{10}y^2 - \frac{11}{10}xy - \frac{39}{20}x^2 + \cdots. \tag{3.9}$$

This completes the proof. □

When $b \in (0.2, 1]$, the characteristic polynomials of the Jacobian matrix of the system at $P_{1,2}$ are given by

$$g_{1,2}(\lambda) = \lambda^3 + p_{1,2}\lambda^2 + q_{1,2}\lambda + r_{1,2}, \tag{3.10}$$

respectively, where

$$p_{1,2} = -\left(5b \pm 6\sqrt{b^2 - 25^{-1}}\right), \tag{3.11}$$

$$q_{1,2} = 0.8 + 5b^2 \pm b\sqrt{25b^2 - 1}, \tag{3.12}$$

$$r_{1,2} = \mp\sqrt{b^2 - 25^{-1}}. \tag{3.13}$$

Since Routh-Hurwitz criteria are not met, we can determine that both the equilibria are unstable. For the first equilibrium P_1, we have $r_1 < 0$, thus this equilibrium is unstable. For the second equilibrium P_2, we have $p_2 q_2 - r_2 < 0$, thus this equilibrium is unstable.

3.3.2. Bifurcation analysis

Figure 12 shows the bifurcation diagram of x for the system, showing the different types of dynamics exhibited by the system depending on the value of b. A reverse period-doubling route to chaos can be observed, which can help understand the hidden chaotic behavior at $b = 0.195$ in subsection 2.3. On the far left of the parameter range $[0, 1]$, the system exhibits a period-3 attractor.

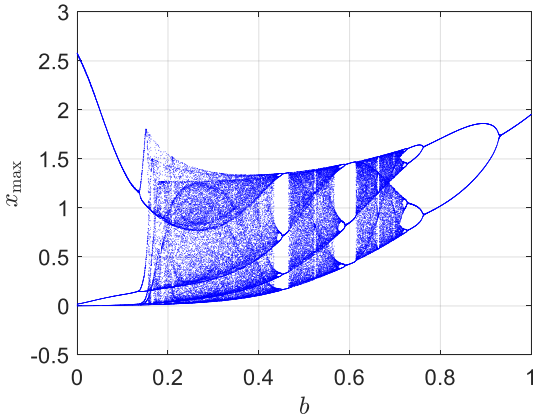

Figure 12. Bifurcation diagram of x for system (2.1) versus the parameter $b \in [0, 1]$ with $\mu(z) = 0.1 - bz + 0.1z^2$ and initial conditions $x(0) = z(0) = 0, y(0) = 1$.

From the Figure 12 and the previous equilibrium analysis, we have the following results. For $0 \le b < 0.2$, the system exhibits a hidden attractor without equilibrium. At $b = 0.2$, the system exhibits a self-excited chaotic attractor with a nonhyperbolic, unstable equilibrium, see Figure 13.

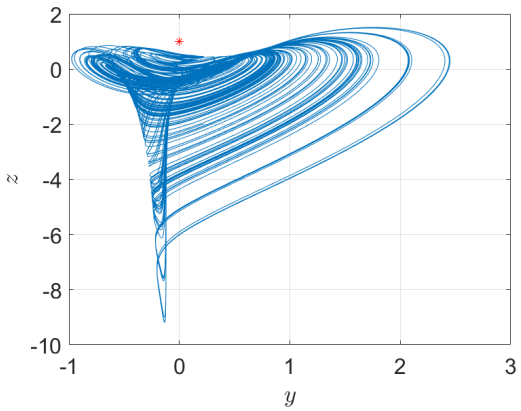

Figure 13. Projection of a self-excited chaotic attractor onto y-z plane for system (2.1) with $\mu(z) = 0.1 - 0.2z + 0.1z^2$ and initial conditions $x(0) = z(0) = 0, y(0) = 1$. Red star: unstable equilibrium at $(0, 0, 1)$.

For $0.2 < b \leq 1$, the system exhibits a self-excited attractor with two unstable equilibria. The parameter value $b = 0.2$ is the threshold between hidden chaos and self-excited chaos.

The Lyapunov exponent spectrum of the system with respect to the parameter b is displayed in Figure 14, which is consistent with the bifurcation diagram shown in Figure 12.

4. Subcritical Hopf bifurcation of system (2.1) with $\mu(z) = a - z$

Consider system (2.1) with the function

$$\mu(z) = a - z.$$

The parameter a is used as the bifurcation parameter. In this scenario, the system exhibits a unique equilibrium point located at $P : (0, 0, a)$.

Theorem 4.1. *Consider system* (2.1) *with the function*

$$\mu(z) = a - z.$$

If $a < 0$, the equilibrium point $P(0, 0, a)$ is locally asymptotically stable. When $-2 < a < 0$, the equilibrium is a stable node-focus. Furthermore, for $a \leq -2$, the equilibrium is a stable node.

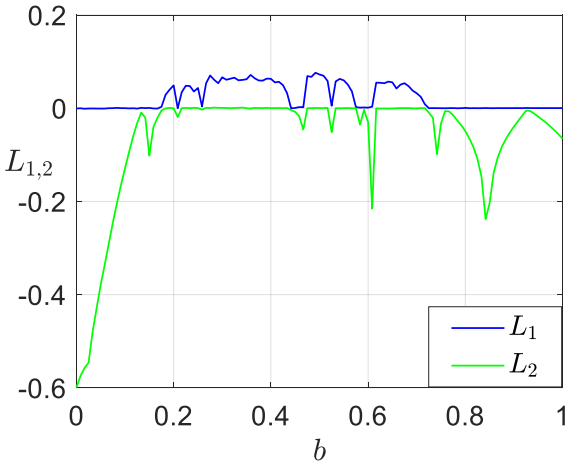

(a) The first two Lyapunov exponents $L_{1,2}$.

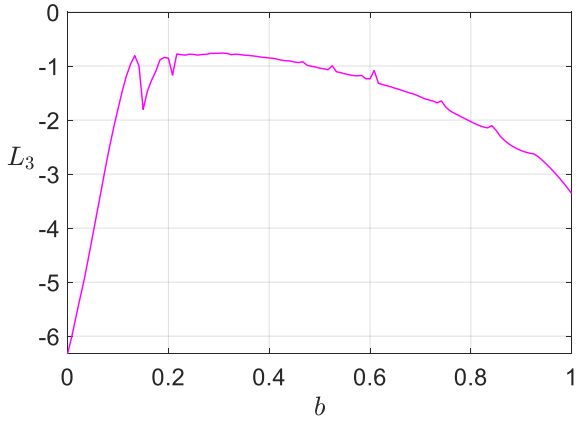

(b) The third Lyapunov exponent L_3.

Figure 14. Lyapunov exponent spectrum of system (2.1) versus the parameter $b \in [0, 1]$ with $\mu(z) = 0.1 - bz + 0.1z^2$ and initial conditions $x(0) = z(0) = 0, y(0) = 1$.

Proof. The Jacobian matrix of the system at the equilibrium P is

$$A = \begin{pmatrix} 0 & 1 & 0 \\ -1 & a & 0 \\ a & 0 & -1 \end{pmatrix}, \tag{4.1}$$

for which the characteristic equation is

$$g(\lambda) = \lambda^3 + (1-a)\,\lambda^2 + (1-a)\,\lambda + 1 = 0. \tag{4.2}$$

Let us introduce some notation

$$\begin{cases} p = \frac{1}{2}\,g''(0), \\ q = g'(0), \\ r = g(0), \\ \delta = p\,q - r, \\ \Delta = -p^2\,q^2 + 4\,p^3\,r + 4\,q^3 - 18\,p\,q\,r + 27\,r^2. \end{cases} \tag{4.3}$$

According to Routh-Hurwitz criterion, the equilibrium is locally asymptotically stable if $p, q, r > 0$ and $\delta > 0$, i.e., $a < 0$. The following assertions are based on [42]. For $-2 < a < 0$, we have $\delta > 0, r > 0, q > 0$ and $\Delta > 0$, thus the equilibrium is a stable node-focus; for $a \le -2$, we have $\delta > 0, r > 0, q > 0$ and $\Delta \le 0$, thus the equilibrium is a stable node. □

Theorem 4.2. *Consider system* (2.1) *with the function* $\mu(z) = a - z$. *In this scenario, as the parameter a passes through zero, a subcritical Hopf bifurcation occurs at the equilibrium* $P\,(0, 0, a)$, *which gives rise to an unstable limit cycle for* $a < 0$. *At* $a = 0$, *the equilibrium located at the origin is unstable.*

Proof. When $a = 0$, the characteristic equation (4.2) has a pair of purely imaginary roots $\lambda_{1,2} = \pm\mathrm{i}$ and $\lambda_3 = -1$. Based on (4.2) and the implicit function theorem, we have

$$\left.\frac{d\lambda}{da}\right|_{a=0,\lambda=\mathrm{i}} = \frac{1}{2}, \tag{4.4}$$

so the transversality condition for the Hopf bifurcation at $a = 0$ is certainly satisfied. According to [43], a Hopf bifurcation occurs at the equilibrium P when the parameter a passes through $a = 0$.

Setting $\mu(z) = -z$, system (2.1) becomes

$$\begin{cases} \dfrac{dx}{dt} = y, \\ \dfrac{dy}{dt} = -x + y\,z, \\ \dfrac{dz}{dt} = -z - 5\,x\,y + x\,z. \end{cases} \tag{4.5}$$

By introducing the transformation

$$\begin{cases} x = (-u + v)\,\mathrm{i}, \\ y = u + v, \\ z = w, \end{cases} \tag{4.6}$$

system (4.5) becomes

$$\begin{cases} \dfrac{du}{dt} = u\,\mathrm{i} + \frac{1}{2}\,(u+v)\,w, \\ \dfrac{dv}{dt} = -v\,\mathrm{i} + \frac{1}{2}\,(u+v)\,w, \\ \dfrac{dw}{dt} = -w + (5\,u + 5\,v - w)(u - v)\,\mathrm{i}. \end{cases} \tag{4.7}$$

For later convenience, let (U, V, W) represent the vector field associated to system (4.7).

According to [44], we can determine a formal series

$$F(u, v, w) = uv + \sum_{\substack{p_1+p_2+q=3 \\ p_1,p_2,q\ge 0}}^{\infty} C_{p_1,p_2,q}\,u^{p_1}v^{p_2}w^q, \tag{4.8}$$

such that

$$\left.\frac{dF}{dt}\right|_{(4.7)} = \frac{\partial F}{\partial u}U + \frac{\partial F}{\partial v}V + \frac{\partial F}{\partial w}W = \sum_{n=1}^{\infty} W_n (uv)^{n+1}, \tag{4.9}$$

where W_n are called the n-th focus quantities of system (4.7).

Here, we only need to compute the first focus quantity. Let

$$\begin{aligned} F(u, v, w) \;=\; & uv + \left(\frac{1}{20} + \frac{\mathrm{i}}{20}\right)u^3w - \frac{5v^3u}{2} + \left(\frac{1}{20} - \frac{\mathrm{i}}{20}\right)v^3w \\ & + \left(\frac{7}{20} - \frac{11\,\mathrm{i}}{20}\right)u^2vw - \frac{5vu^3}{2} + \left(\frac{1}{10} + \frac{\mathrm{i}}{5}\right)u^2w \\ & + \frac{3w^2vu}{5} + \left(-\frac{1}{8} + \frac{\mathrm{i}}{4}\right)v^4 + \left(\frac{1}{10} - \frac{\mathrm{i}}{5}\right)v^2w^2 \\ & + wvu + \left(\frac{1}{10} - \frac{\mathrm{i}}{5}\right)v^2w + \left(\frac{1}{10} + \frac{\mathrm{i}}{5}\right)u^2w^2 \\ & - \left(\frac{1}{8} + \frac{\mathrm{i}}{4}\right)u^4 + \left(\frac{7}{20} + \frac{11\,\mathrm{i}}{20}\right)u\,v^2w + \cdots, \end{aligned} \tag{4.10}$$

we find that

$$\left.\frac{dF}{dt}\right|_{(4.7)} = 2\,(uv)^2 + \cdots, \tag{4.11}$$

and thus

$$W_1 = 2. \tag{4.12}$$

Based on the signs of (4.4) and (4.12), we can conclude that the Hopf bifurcation in the system is subcritical, resulting in the emergence of a single unstable limit cycle for $a < 0$; at $a = 0$, the equilibrium located at the origin is unstable. □

5. Electronic circuit design and simulation with Multisim

Chaos circuits play a crucial role across diverse application domains, notably in ensuring secure communication and image encryption [45, 46]. The design and simulation of chaotic circuits are crucial in validating chaotic systems. Multisim is a simulation tool designed specifically to help create and test analog and digital circuits on circuit boards.

In order to validate the dynamics of the hidden chaotic system

$$\begin{cases} \dfrac{dx}{d\tau} = y, \\ \dfrac{dy}{d\tau} = -x + y\,z, \\ \dfrac{dz}{d\tau} = 0.1 - 0.195\,z + 0.1\,z^2 - 5\,x\,y + x\,z, \end{cases} \tag{5.1}$$

with the initial conditions $x(0) = z(0) = 0$ and $y(0) = 1$, a circuit realization of the system is designed and simulated in the Multisim 14.

The electronic circuit, designed for the implementation of the system (5.1), is shown in Figure 15. The setup of this circuit is accomplished using Multisim. It consists of four operational amplifiers U_i ($i = 1, 2, 3, 4$, using AD711JN) powered at ± 15 V, three capacitors C_i ($i = 1, 2, 3$) of 100nF, and ten resistors R_i ($i = 1, 2, \cdots, 10$) with

$$R_1 = R_2 = R_3 = R_5 = R_6 = R_8 = R_9 = R_{10} = 10\text{k}\Omega,$$

$$R_4 = 2\text{k}\Omega, \quad R_7 = 51.282\text{k}\Omega.$$

By applying Kirchhoff's circuit laws to the circuit shown in Figure 15, we get the following circuital system

$$\begin{cases} RC\dfrac{dx}{dt} = \dfrac{R}{R_1}\,y, \\ RC\dfrac{dy}{dt} = -\dfrac{R}{R_2}\,x + \dfrac{R}{R_3}\,y\,z, \\ RC\dfrac{dz}{dt} = \dfrac{R}{R_6}\,V_0 - \dfrac{R}{R_7}\,z + \dfrac{0.1\,R}{R_8}\,z^2 \\ \qquad\quad -\dfrac{R}{R_4}\,x\,y + \dfrac{R}{R_5}\,x\,z. \end{cases} \tag{5.2}$$

Here

$$dt = RC\,d\tau, \quad R = 10\text{k}\Omega, \quad C = 10\text{nF}, \quad V_0 = 0.1\text{V}.$$

The variables x, y, z denote the output voltages of capacitors C_1, C_2 and C_3, respectively. The initial conditions are

$$x(0) = z(0) = 0\text{V}, \; y(0) = 1\text{V}.$$

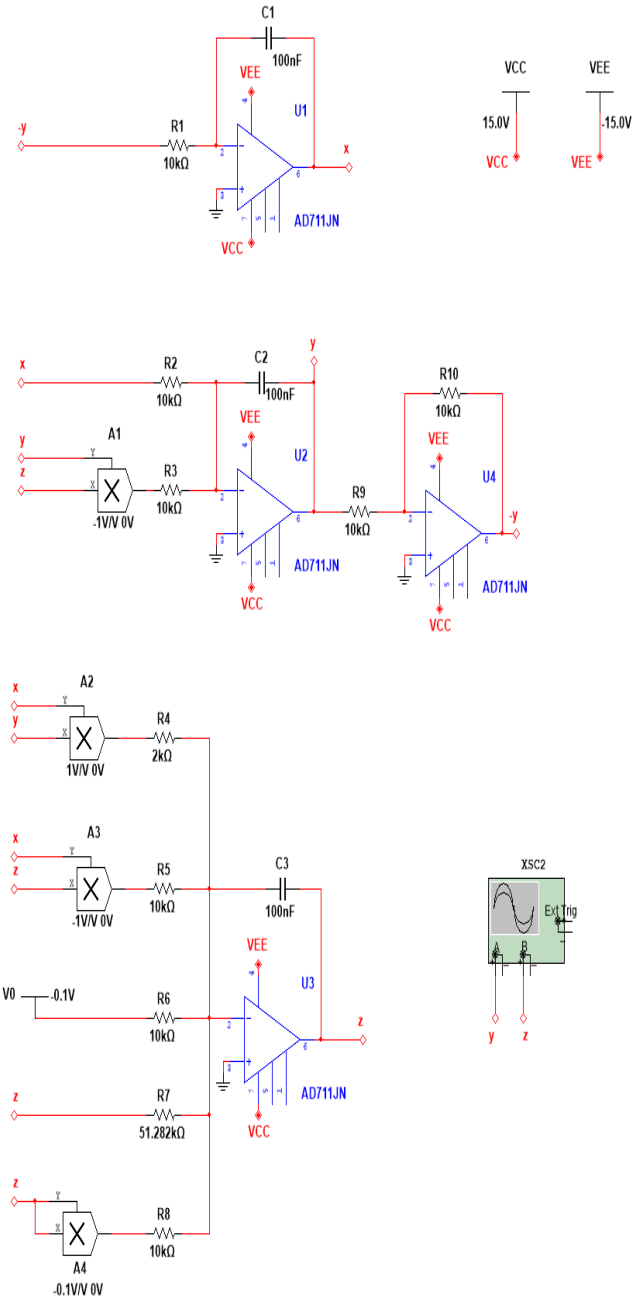

Figure 15. Schematic diagram of the electronic circuit of the hidden chaotic system (5.2).

Using Multisim simulation, three 2D projections of the hidden chaotic attractor of system (5.2) observed from the

oscilloscope are shown in Figure 16. The outcomes of the circuit modeling align well with Figure 5, demonstrating the soundness and feasibility of the proposed system (5.1).

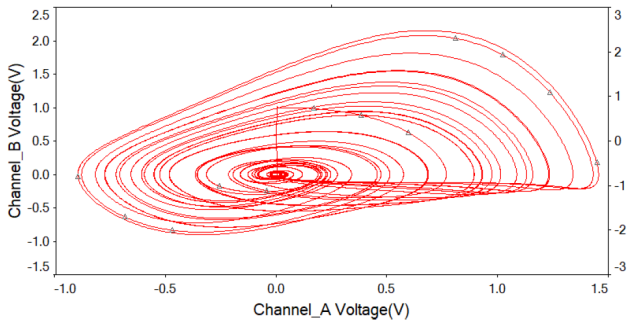

(a) x-y plane

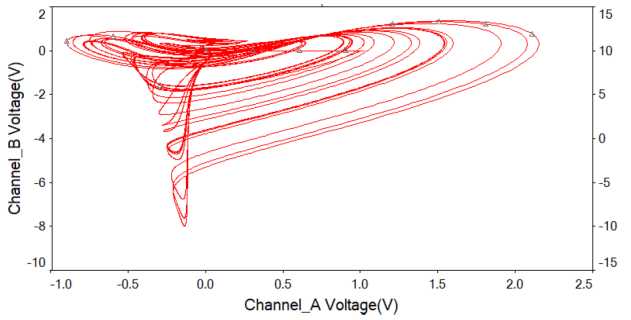

(b) y-z plane

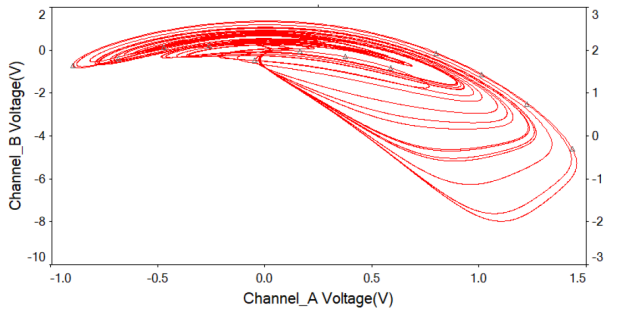

(c) x-z plane

Figure 16. Different 2D projections of the hidden chaotic attractor (without equilibrium) of system (5.2) for the initial conditions $x(0) = z(0) = 0$V and $y(0) = 1$V.

6. Conclusions

In this work, we have proposed a quadratic family of chameleon chaotic systems with a function $\mu(z)$. The dynamics exhibited by the system are significantly influenced by the form of the function $\mu(z)$. Different forms of $\mu(z)$, including linear, quadratic, and affine expressions, are explored. If $\mu(z)$ assumes a linear form, the system can exhibit a self-excited attractor, coexisting with an unstable nonhyperbolic equilibrium point. When $\mu(z)$ is in an affine form, the system can demonstrate a hidden chaotic attractor, coexisting with a stable hyperbolic equilibrium point. When $\mu(z)$ is in a quadratic form, the system can display a hidden chaotic attractor without any equilibrium points or a self-excited chaotic attractor with two unstable equilibrium points. By varying the linear coefficient in $\mu(z)$, we investigate the creation of self-excited and hidden attractors. This lets us understand how attractors change. We use Hopf bifurcation analysis and numerical tools like bifurcation diagrams, phase portraits, Lyapunov exponents, and basins of attraction.

Finally, an electronic circuit is designed and simulated using Multisim to realize a hidden chaotic system with no equilibrium points. The simulations exhibit favorable agreement with the theoretical model, thereby offering an experimental validation of the hidden chaotic system. In conclusion, this paper affirms that quadratic systems can generate different types of chaos through period-doubling routes. In the future, we will develop some chameleon systems that incorporate piecewise, trigonometric, hyperbolic, or absolute value functions. These systems may exhibit various routes to chaos, such as period-doubling route, intermittent route, and quasi-periodic route. We hope this will enhance our comprehension of the relation between self-excited and hidden attractors.

Use of AI tools declaration

The authors declare they have not used Artificial Intelligence (AI) tools in the creation of this paper.

Acknowledgments

This research is supported by the Shandong Provincial Natural Science Foundation (No. ZR2018MA025).

Author contributions

Conceptualization, Xue Zhang; methodology, Bingxue Li; software, Jie Liu, Lihua Fan, Ning Wang; writing-original draft preparation, Xue Zhang; writing-review and editing, Bo Sang, Xue Zhang.

Conflict of interest

All authors declare no conflicts of interest in this paper.

References

1. V. G. Ivancevic, T. T. Ivancevic, *Quantum neural computation*, New York: Springer, 2010. http://doi.org/10.1007/978-90-481-3350-5
2. D. Toker, F. T. Sommer, M. D'Esposito, A simple method for detecting chaos in nature, *Commun. Biol.*, **3** (2020), 11. http://doi.org/10.1038/s42003-019-0715-9
3. H. W. Lorenz, *Nonlinear dynamical economics and chaotic motion*, Berlin: Springer, 1993. http://doi.org/10.1007/978-3-642-78324-1
4. S. Lundqvist, N. H. March, M. P. Tosi, *Order and chaos in nonlinear physical systems*, New York: Springer, 1988. http://doi.org/10.1007/978-1-4899-2058-4
5. Q. Lai, B. Bao, C. Chen, J. Kengne, A. Akgul, Circuit application of chaotic systems: modeling, dynamical analysis and control, *Eur. Phys. J. Spec. Top.*, **230** (2021), 1691–1694. http://doi.org/10.1140/epjs/s11734-021-00202-0
6. N. Wang, D. Xu, N. V. Kuznetsov, H. Bao, M. Chen, Q. Xu, Experimental observation of hidden Chua's attractor, *Chaos Solitons Fract.*, **170** (2023), 113427. http://doi.org/10.1016/j.chaos.2023.113427
7. N. V. Kuznetsov, G. A. Leonov, V. I. Vagaitsev, Analytical-numerical method for attractor localization of generalized Chua's system, *IFAC Proc. Vol.*, **43** (2010), 29–33. http://doi.org/10.3182/20100826-3-TR-4016.00009
8. G. A. Leonov, N. V. Kuznetsov, V. I. Vagaitsev, Localization of hidden Chua's attractors, *Phys. Lett. A*, **375** (2011), 2230–2233. http://doi.org/10.1016/j.physleta.2011.04.037
9. G. A. Leonov, N. V. Kuznetsov, V. I. Vagaitsev, Hidden attractor in smooth Chua systems, *Phys. D*, **241** (2012), 1482–1486. http://doi.org/10.1016/j.physd.2012.05.016
10. S. Jafari, J. C. Sprott, F. Nazarimehr, Recent new examples of hidden attractors, *Eur. Phys. J. Spec. Top.*, **224** (2015), 1469–1476. http://doi.org/10.1140/epjst/e2015-02472-1
11. Z. Wang, Z. Wei, K. Sun, S. He, H. Wang, Q. Xu, et al., Chaotic flows with special equilibria, *Eur. Phys. J. Spec. Top.*, **229** (2020), 905–919. http://doi.org/10.1140/epjst/e2020-900239-2
12. X. Wang, N. V. Kuznetsov, G. Chen, *Chaotic systems with multistability and hidden attractors*, Switzerland: Springer, 2021. http://doi.org/10.1007/978-3-030-75821-9
13. N. Kuznetsov, T. Mokaev, V. Ponomarenko, E. Seleznev, N. Stankevich, L. Chua, Hidden attractors in Chua circuit: mathematical theory meets physical experiments, *Nonlinear Dyn.*, **111** (2023), 5859–5887. http://doi.org/10.1007/s11071-022-08078-y
14. Z. Wang, A. Ahmadi, H. Tian, S. Jafari, G. Chen, Lower-dimensional simple chaotic systems with spectacular features, *Chaos Solitons Fract.*, **169** (2023), 113299. http://doi.org/10.1016/j.chaos.2023.113299
15. G. A. Leonov, N. V. Kuznetsov, On differences and similarities in the analysis of Lorenz, Chen, and Lu systems, *Appl. Math. Comput.*, **256** (2015), 334–343. http://doi.org/10.1016/j.amc.2014.12.132
16. G. A. Leonov, N. V. Kuznetsov, Hidden attractors in dynamical systems: systems with no equilibria, multistability and coexisting attractors, *IFAC Proc. Vol.*, **47** (2014), 5445–5454. http://doi.org/10.3182/20140824-6-ZA-1003.02501
17. D. Dudkowski, A. Prasad, T. Kapitaniak, Perpetual points: new tool for localization of co-existing attractors in dynamical systems, *Int. J. Bifurcat. Chaos*, **27** (2017), 1750063. http://doi.org/10.1142/S0218127417500638
18. D. Dudkowski, A. Prasad, T. Kapitaniak, Perpetual points and hidden attractors in dynamical systems, *Phys. Lett. A*, **379** (2015), 2591–2596. http://doi.org/10.1016/j.physleta.2015.06.002

19. F. Nazarimehr, B. Saedi, S. Jafari, J. C. Sprott, Are perpetual points sufficient for locating hidden attractors? *Int. J. Bifurcat. Chaos*, **27** (2017), 1750037. http://doi.org/10.1142/S0218127417500377

20. X. Wang, Ü. Çavuşoğlu, S. Kacar, A. Akgul, V. T. Pham, S. Jafari, et al., S-box based image encryption application using a chaotic system without equilibrium, *Appl. Sci.*, **9** (2019), 781. http://doi.org/10.3390/app9040781

21. X. Wang, G. Chen, A chaotic system with only one stable equilibrium, *Commun. Nonlinear Sci. Numer. Simul.*, **17** (2012), 1264–1272. http://doi.org/10.1016/j.cnsns.2011.07.017

22. S. Jafari, J. C. Sprott, Simple chaotic flows with a line equilibrium, *Chaos Solitons Fract.*, **57** (2013), 79–84. http://doi.org/10.1016/j.chaos.2013.08.018

23. V. T. Pham, C. Volos, S. Jafari, Z. Wei, X. Wang, Constructing a novel no-equilibrium chaotic system, *Int. J. Bifurcat. Chaos*, **24** (2014), 1450073. http://doi.org/10.1142/S0218127414500734

24. V. T. Pham, S. Jafari, T. Kapitaniak, Constructing a chaotic system with an infinite number of equilibrium points, *Int. J. Bifurcat. Chaos*, **26** (2016), 1650225. http://doi.org/10.1142/S0218127416502254

25. V. T. Pham, S. Jafari, T. Kapitaniak, C. Volos, S. T. Kingni, Generating a chaotic system with one stable equilibrium, *Int. J. Bifurcat. Chaos*, **27** (2017), 1750053. http://doi.org/10.1142/S0218127417500535

26. M. A. Jafari, E. Mliki, A. Akgul, V. T. Pham, S. T. Kingni, X. Wang, et al., Chameleon: the most hidden chaotic flow, *Nonlinear Dyn.*, **88** (2017), 2303–2317. http://doi.org/10.1007/s11071-017-3378-4

27. F. Wu, T. Hayat, X. An, J. Ma, Can Hamilton energy feedback suppress the chameleon chaotic flow? *Nonlinear Dyn.*, **94** (2018), 669–677. http://doi.org/10.1007/s11071-018-4384-x

28. S. Mobayen, A. Fekih, S. Vaidyanathan, A. Sambas, Chameleon chaotic systems with quadratic nonlinearities: an adaptive finite-time sliding mode control approach and circuit simulation, *IEEE Access*, **9** (2021), 64558–64573. http://doi.org/10.1109/ACCESS.2021.3074518

29. C. Li, J. C. Sprott, Multistability in a butterfly flow, *Int. J. Bifurcat. Chaos*, **23** (2013), 1350199. http://doi.org/10.1142/S021812741350199X

30. A. N. Pisarchik, U. Feudel, Control of multistability, *Phys. Rep.*, **540** (2014), 167–218. http://doi.org/10.1016/j.physrep.2014.02.007

31. T. Kapitaniak, G. A. Leonov, Multistability: uncovering hidden attractors, *Eur. Phys. J. Spec. Top.*, **224** (2015), 1405–1408. http://doi.org/10.1140/epjst/e2015-02468-9

32. P. R. Sharma, M. D. Shrimali, A. Prasad, N. V. Kuznetsov, G. A. Leonov, Control of multistability in hidden attractors, *Eur. Phys. J. Spec. Top.*, **224** (2015), 1485–1491. http://doi.org/10.1140/epjst/e2015-02474-y

33. A. Ahmadi, S. Parthasarathy, H. Natiq, S. Jafari, I. Franović, K. Rajagopal, A non-autonomous mega-extreme multistable chaotic system, *Chaos Solitons Fract.*, **174** (2023), 113765. http://doi.org/10.1016/j.chaos.2023.113765

34. T. Moalemi, A. Ahmadi, S. Jafari, G. Chen, A novel mega-stable system with attractors in real-life object shapes, *Sci. Iran.*, in press, 2023. http://doi.org/10.24200/SCI.2023.60858.7030

35. R. Zhou, Y. Gu, J. Cui, G. Ren, S. Yu, Nonlinear dynamic analysis of supercritical and subcritical Hopf bifurcations in gas foil bearing-rotor systems, *Nonlinear Dyn.*, **103** (2021), 2241–2256. http://doi.org/10.1007/s11071-021-06234-4

36. N. V. Stankevich, N. V. Kuznetsov, G. A. Leonov, L. O. Chua, Scenario of the birth of hidden attractors in the Chua circuit, *Int. J. Bifurcat. Chaos*, **27** (2017), 1730038. http://doi.org/10.1142/S0218127417300385

37. H. Zhao, Y. Lin, Y. Dai, Hopf bifurcation and hidden attractor of a modified Chua's equation, *Nonlinear Dyn.*, **90** (2017), 2013–2021. http://doi.org/10.1007/s11071-017-3777-6

38. M. Liu, B. Sang, N. Wang, I. Ahmad, Chaotic dynamics by some quadratic jerk systems, *Axioms*, **10** (2021), 227. http://doi.org/10.3390/axioms10030227

39. B. Li, B. Sang, M. Liu, X. Hu, X. Zhang, N. Wang, Some jerk systems with hidden chaotic dynamics, *Int. J. Bifurcat. Chaos*, **33** (2023), 2350069. http://doi.org/10.1142/S0218127423500694

40. S. Kumarasamy, M. Banerjee, V. Varshney, M. D. Shrimali, N. V. Kuznetsov, A. Prasad, Saddle-node bifurcation of periodic orbit route to hidden attractors, *Phys. Rev. E*, **107** (2023), L052201. http://doi.org/10.1103/PhysRevE.107.L052201
41. A. Wolf, J. B. Swift, H. L. Swinney, J. A. Vastano, Determining Lyapunov exponents from a time series, *Phys. D*, **16** (1985), 285–317. http://doi.org/10.1016/0167-2789(85)90011-9
42. I. N. Bronshtein, K. A. Semendyayev, G. Musiol, H. Mühlig, *Handbook of mathematics*, Berlin: Springer, 2015. http://doi.org/10.1007/978-3-662-46221-8
43. W. Liu, Criterion of Hopf bifurcations without using eigenvalues, *J. Math. Anal. Appl.*, **182** (1994), 250–256. http://doi.org/10.1006/jmaa.1994.1079
44. B. Sang, B. Huang, Bautin bifurcations of a financial system, *Electron. J. Qual. Theory Differ. Equations*, **95** (2017), 1–22. http://doi.org/10.14232/ejqtde.2017.1.95
45. B. Zhang, L. Liu, Chaos-based image encryption: review, application, and challenges, *Mathematics*, **11** (2023), 2585. http://doi.org/10.3390/math11112585
46. A. Noor, Z. G. Ç. Taşkıran, Random number generator and secure communication applications based on infinitely many coexisting chaotic attractors, *Electrica*, **21** (2021), 180–188. http://doi.org/10.5152/electrica.2021.21017

AIMS Press